Chapter 6

Developing a Hybrid Model and a Multi-Scale 3D Concept of Integrated Modelling High-Temperature Processes

Marcin Hojny

Additional information is available at the end of the chapter

http://dx.doi.org/10.5772/67735

Abstract

The chapter presents an idea of constructing a scientific workshop focused on high-temperature processes, based upon a concept of integrated modelling combining the advantages of computer and physical simulations. Examples of physical simulation results aiming at determining necessary material data and high-temperature characteristics for the needs of computer simulations are presented. They are complemented by an outline of numerical 3D models developed and results of test simulations of a 3D solver of the finite element method (FEM) and the smoothed particle hydrodynamics (SPH). This chapter is closed with a short summary, indicating trends in further research focused on a further development of the DEFFEM simulation package and research and measurement methods.

Keywords: extra-high temperature, finite element method (FEM), smoothed particle hydrodynamics (SPH), physical simulation, computer simulation, mushy zone

1. Introduction

In recent years, many companies have been working to develop a rolling process with the semi-solid core [1–6]. While thin strip casting combined with subsequent rolling is a simple, improved method of the conventional rolling process, rolling a strip, in which both the solid and liquid phases coexist, is a new process. Cold rolling following simple strand casting is a long process and it is not cost-effective because of energy reasons. For technological reasons, the process should be developed to simplify or eliminate some operations, which would drastically reduce the energy costs. This also involves beneficial environmental impact, due to the reduction of gas emissions. Casting processes followed immediately by rolling have various versions, which depend on the applying companies, and differ with details of industrial installations [7]. However, the need for controlled rolling of strands cast is pointed out.

Therefore, results of a computer simulation or a physical simulation of the process analysed will be useful to control the process parameters. This has inspired the author to take up intensive and time-consuming work related to the development of research methods and mathematical models, along with their numerical implementation [7]. The research and scientific work carried out since 2009 as part of two projects financed by Polish academic institutions resulted in the development of modelling concepts integrating physical and computer simulation areas, while providing full or partial exchange of information between those areas. The proposed concept utilizes capabilities of modern thermomechanical simulators of the Gleeble 3800 series in the modelling of steel deformation processes at extra-high temperatures, as well as in the modelling of integrated casting and rolling processes of flat strands with a solidifying core. The other necessary and unique component in the global scale is the original simulation package DEFFEM being developed for a few years, dedicated to two classes of issues, namely the processes of steel deformation modelling within a temperature range near the solidus line, and within a temperature range between the solidus and liquidus temperatures. The mentioned two classes of issues have been jointly classified as high-temperature processes. The whole modelling approach is complemented by the utilisation of modern testing and measurement instruments to verify the implemented solutions or to obtain additional information that cannot be obtained with traditional methods. This required adopting a number of simplifications and assumptions. Most important was systematic pursuit of the assumed goals and recent research in the context of planned work aiming at developing two unique numerical models: a full three-dimensional multi-scale model MCFE (Monte Carlo and finite elements) and a hybrid model combining the advantages of the finite element method (FEM) and the smoothed particle hydrodynamics (SPH). The author's research is therefore pioneering both in theory and practice. The general outline of the developed concept is presented in **Figure 1**. Coupling and exchange of information

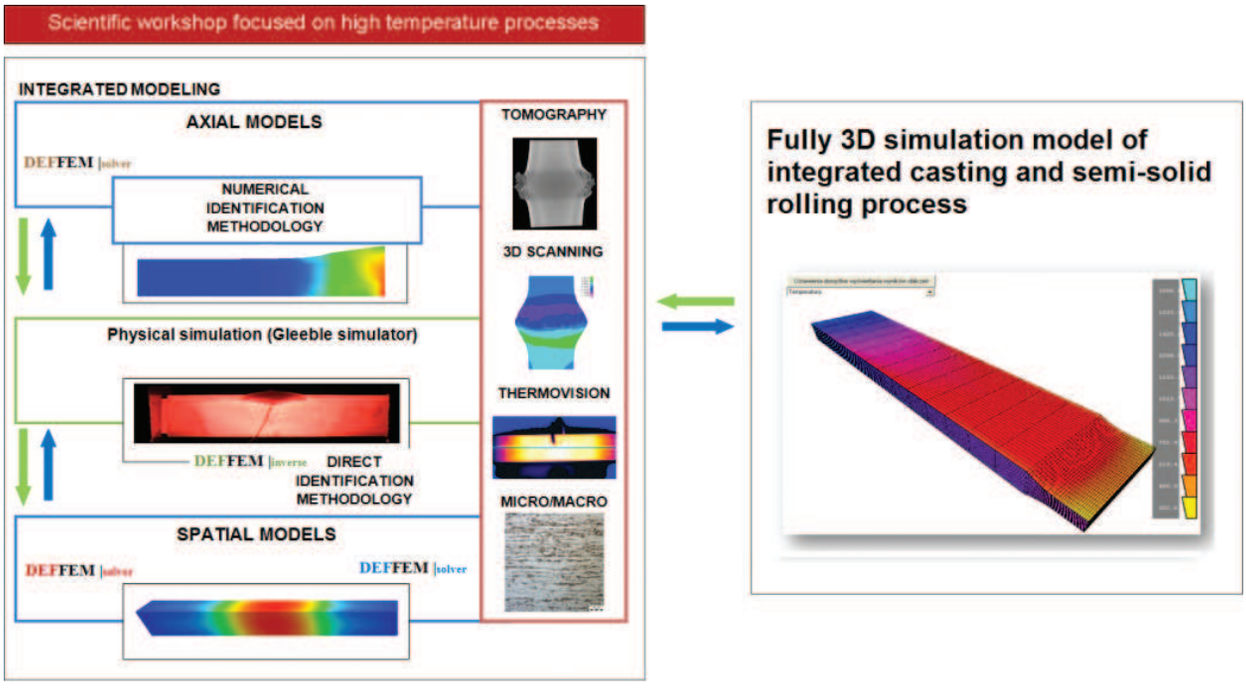

Figure 1. General outline of the concept of integrated modelling focused on high-temperature processes.

http://dx.doi.org/10.5772/67735

between the areas of physical and computer simulations allows, among others, the necessary data for the needs of numerical simulations (stress-strain curves, characteristics of changes of current intensity versus time, local temperature changes within the sample volume, etc.) to be identified. At the same time, the application of computer simulations using the dedicated simulation system DEFFEM allows the obtained physical simulation findings to be interpreted [7]. A few layers can be specified when analysing the general outline of the concept in **Figure 1**. The foundation constitutes axisymmetrical solutions, being a key to the developed NIM (numerical identification methodology) for determining mechanical properties of the steels tested, necessary for numerical analyses. Regardless of axisymmetrical solutions, the next layer constitutes 3D solutions, which become important in the context of designing the simulation system of integrated strip casting and rolling. Such approach is determined by the fact that the zone of solid and liquid phases mixing within the volume of the strand rolled often has a very irregular shape [7].

More details concerning the developed concept of integrated modelling or comprehensive physical tests can be found in the recapitulating monograph by Hojny [7].

2. The DEFFEM simulation system

The original simulation package DEFFEM is developed in accordance with the design philosophy **ONEDES** (**ONEDE**Cision**S**oftware) proposed by Hojny [8]. It is based on the assumption that a set of independent modules comprising the DEFFEM package is implemented numerically to enable a virtual test of resistance heating combined with deforming in a wide range of temperatures to be performed, in particular at extra-high temperatures near the solidus line, as well as in conditions of the solid and liquid phase coexistence, without the need for any commercial applications. In **Table 1** currently developed modules (solvers) are compared with the ones under development included in the DEFFEM package, along with their classification subject to the adopted numerical simulations (solver class) and the very possibilities for using the solver to simulate specific main features. The developed simulation

Module	Solver class	Main features
DEFFEM |solver_2D_TH v.1.0	2D thermal, finite element method	• Convection heat transfer • Transient heat flow
DEFFEM |solver_AX_TH v.1.0	Axially symmetric, thermal, finite element method	• Convection heat transfer • Transient heat flow • Resistance heating
DEF_SEMI_SOLID v. 5.0	Axially symmetric, thermo-mechanical, finite element method	• Compression tests • Integrated with magnetohydrodynamic module (MHD) ANSYS software
DEFFEM |solver_AX_TM v. 2.0		• Tension tests • Soft reduction simulation and rolling

Module	Solver class	Main features
		• Integrated with temperature field after resistance heating with DEFFEM |solver_AX_TH
DEFFEM |solver_3D_TH v.1.0	3D thermal, finite element method	• Convection heat transfer • Transient heat flow • Resistance heating
DEFFEM |solver_3D_TM v.1.0	3D thermomechanical, finite element method	• Compression tests • Solidification
DEFFEM |solver_3D_MCFE Beta version	3D multi-scale thermomechanical, Monte Carlo + finite element method	• Compression tests • Solidification
DEFFEM |solver_3D_FLUID v. 1.0	3D fluid, meshless method	• Viscosity • Porous structure • Solidification
DEFFEM |solver_3D_HYBRID Beta version	3D fluid, meshless method +finite element method	• Solidification
Supporting module	Main features	
DEFFEM |pre&post	Full pre- and post-processor for all solvers	
DEFFEM |inverse	Stand-alone inverse module	

Table 1. Component modules of the DEFFEM simulation package.

package also provides tools oriented at the full identification of the selected parameters of numerical models on the basis of data coming directly from physical simulations (**DEFFEM | inverse** module). In parallel with the design of such an advanced simulation tool, the development of visualisation tools and the analysis of findings are being implemented. Advanced numerical algorithms have been developed for plotting the isolines of scalar fields, visualising vector fields or enabling stereoscopic data to be visualised (module **DEFFEM |pre&post**).

3. High-temperature testing methodology

The testing methodology is illustrated with the currently newly tested steel 11SMn30. According to the adopted concept of integrated modelling, physical simulations are performed with a thermomechanical Gleeble 3800 simulator. **Figure 2A** presents a view of the simulation system before starting the physical simulation. During the tests, cylindrical samples (**Figure 2B/C**) and hexahedral samples (**Figure 2D**) with various dimensions were used, along with copper grips with a long zone of contact with the sample (**Figure 2B**).

http://dx.doi.org/10.5772/67735

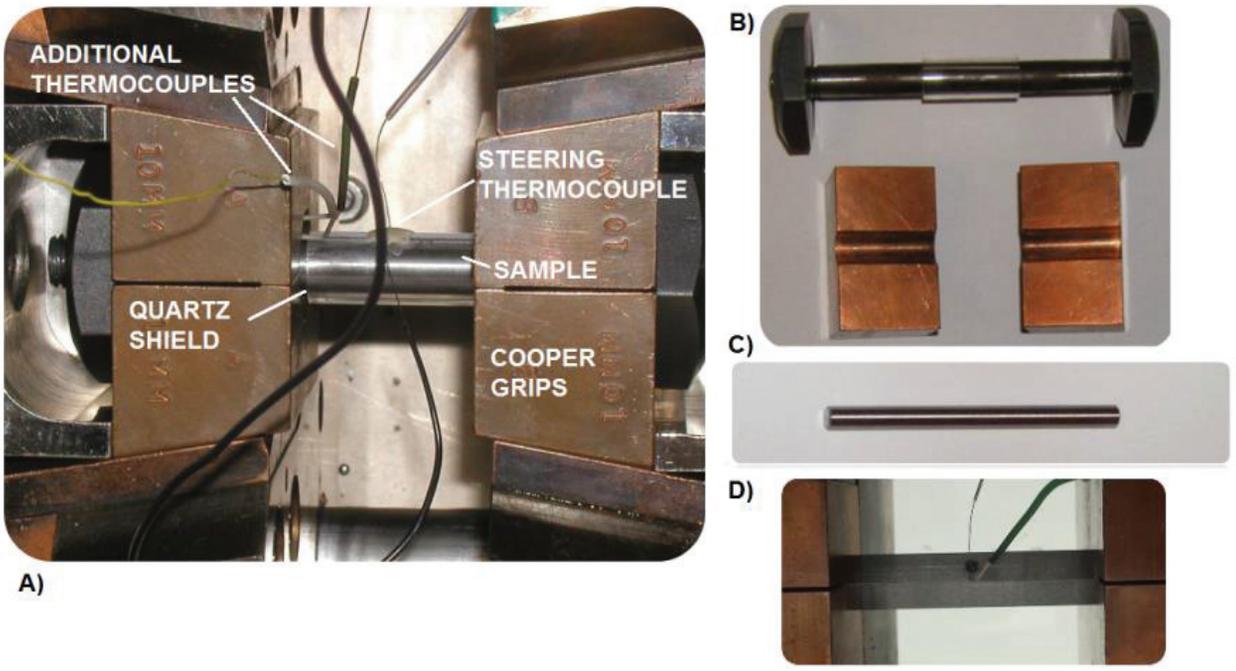

Figure 2. The view of the Gleeble simulator system (A), a cylindrical sample and 'cold' grips (B), a sample for testing the nil strength temperature (NST)(C), and the view of the installed hexahedral sample in the Gleeble simulator system (D).

For the execution of the remelting process, additionally a cylindrical quartz shield was applied to prevent potential leakages of liquid steel into the simulator. To carry out numerical simulations, it was necessary to define material properties characterising the specific steel grade. To determine the necessary thermophysical data, a commercial program JMatPro was used. This program determines the requested dependences (resistivity, thermal conductivity and specific heat) on temperature based on the chemical composition. In order to transfer the simulation results into the industrial conditions, a number of ideas and parameters were introduced to characterise mechanical properties of steel in the semi-solid state. As the 'semi-solid state' we refer hereinafter to the material state able to withstand loads (where within a cohesive solid phase skeleton also the liquid phase coexists). The basic high-temperature characteristics include:

1. Nil strength temperature (NST), at which the material strength determined during steel heating drops to zero. This temperature is determined after applying a very small tensile force, which for the tests carried out with the Gleeble 3800 simulator is about 80 N.

2. Strength recovery temperature (SRT), at which the material regains its strength (>0.05 kg/mm^2 = 0.4909 MPa). It is determined during cooling after previous heating of steel to the liquid state.

3. Nil ductility temperature (NDT), at which ductility determined by reduction of area drops to zero. This temperature is determined during steel heating.

4. Ductility recovery temperature (DRT), at which the reduction of area achieves the value of ≥5%. The temperature DRT is determined during cooling from a temperature over NDT.

5. The determination of changes of stress versus strain on the basis of tensile tests for the selected temperature range and the tool stroke rate.

The tests were carried out on plain samples Ø6 × 82 mm and two-sided threaded samples Ø10 mm × 125 mm. On the basis of computation results based on chemical composition, carried out with the JMatPro program, the calculated liquidus T_l and solidus T_s temperatures were 1518 and 1439°C, respectively. When determining the temperature NST, initially two tests are made. If the difference between the obtained values NST is >20°C, then the third test should be performed. The average value is the temperature NST. In this study, the temperature NST was arbitrary assumed as the mean value for seven samples. The samples for the determination of the nil strength temperature NST first were heated at a rate of 20°C/s to a temperature of 1350°C, and next at a rate of 1°C/s to the temperature of failure. The determined temperature NST for steel 11SMn30 was 1410 ±15°C. The next stage of tests of steel 11SMn30 included determining the nil ductility temperature NDT. The samples for the determination of the nil ductility temperature NDT first were heated at a rate of 20°C/s to a temperature of 1300°C, and next at a rate of 1°C/s to the deformation temperature, using additional 5 s holding at a constant temperature before the deformation process. The samples were tensioned at a rate of 20 mm/s. In steel 11SMn30, the loss of reduction of area was recorded after exceeding the temperature of 1425°C; therefore, it was the temperature NDT. The ductility recovery temperature DRT was determined by heating samples to a temperature of 1300°C at a rate of 20°C/s, and next at a rate of 1°C/s to a temperature of 1425°C. After 5 s of temperature equalisation, the samples were cooled to the deformation temperature, which was between 1370 and 1420°C. The cooling rate was 1°C/s. The deformation was preceded by 5 s holding at a set deformation temperature. The samples were tensioned to failure at a rate of 20 mm/s. The temperature DRT value is determined when 5% of reduction of area is recovered. In steel 11SMn30, the reduction of area of 5% was recorded (when cooled) at a deformation temperature of 1400°C, therefore it is the temperature DRT. The temperature range between NST and DRT is considered the brittle temperature range [7]. For the steel tested the brittle temperature range (BRT) is about 25°C (at a tensioning rate 20 mm/s). The strength recovery temperature SRT was determined by heating samples to a temperature of 1350°C at a rate of 20°C/s, and next at a rate of 1°C/s to a temperature of 1460°C (with zonal sample remelting). After 30 s of holding, the samples were cooled to the deformation temperature, which was between 1400 and 1460°C. The cooling rate was 10°C/s. The deformation was preceded by 5 s holding at a set deformation temperature. The samples were tensioned to failure at a rate of 20 mm/s. The temperature SRT value was determined when a stress of about 0.49 MPa had been recovered. For the conducted tests for steel 11SMn30, it corresponded to the temperature of about 1455°C. At determining the stress value, a correction was applied, namely 60 N was deducted from the maximum force value. This correction was related to overcoming the mechanical system resistance to motion. The knowledge of characteristic temperatures also allows us to determine the steel susceptibility to fracture, which is characterised by the following fracture resistance indicator R_f:

http://dx.doi.org/10.5772/67735

$$R_f = \frac{\text{NST} - \text{NDT}}{\text{NDT}} \tag{1}$$

When the condition NST − NDT < 20C is met, it is assumed that no fracture occurs in steels. As the assumed extreme bottom temperature NST for the steel 11SMn30 tested was 1395°C, the above condition was not met. It indicates that the cast strand shell can break during its formation within the mould, and within the secondary cooling zone. Therefore, we can suppose that this steel is characterised by a high susceptibility to fracture. From the perspective of numerical simulations, the issue of developing a function describing changes in stress versus strain, strain rate and the test nominal temperature becomes very important. The relationships of changes in stress versus strain were determined on the basis of tensile tests. In the experiment, a cylindrical sample was heated to a temperature of 1380°C at a rate of 20°C/s and next at a rate of 1°C/s to 1460°C. The last stage was cooling at a rate of 10°C/s to the deformation temperature. The samples were deformed within the temperature range of 1200–1460°C at three various tool stroke rates of 1, 20 and 100 mm/s.

Figures 3 and **4** present the stress-strain curves obtained directly from the experiment for two various tool stroke rates. The issues of determining the mentioned relationships are complex due to the fact that the temperature field within the sample volume is highly heterogeneous.

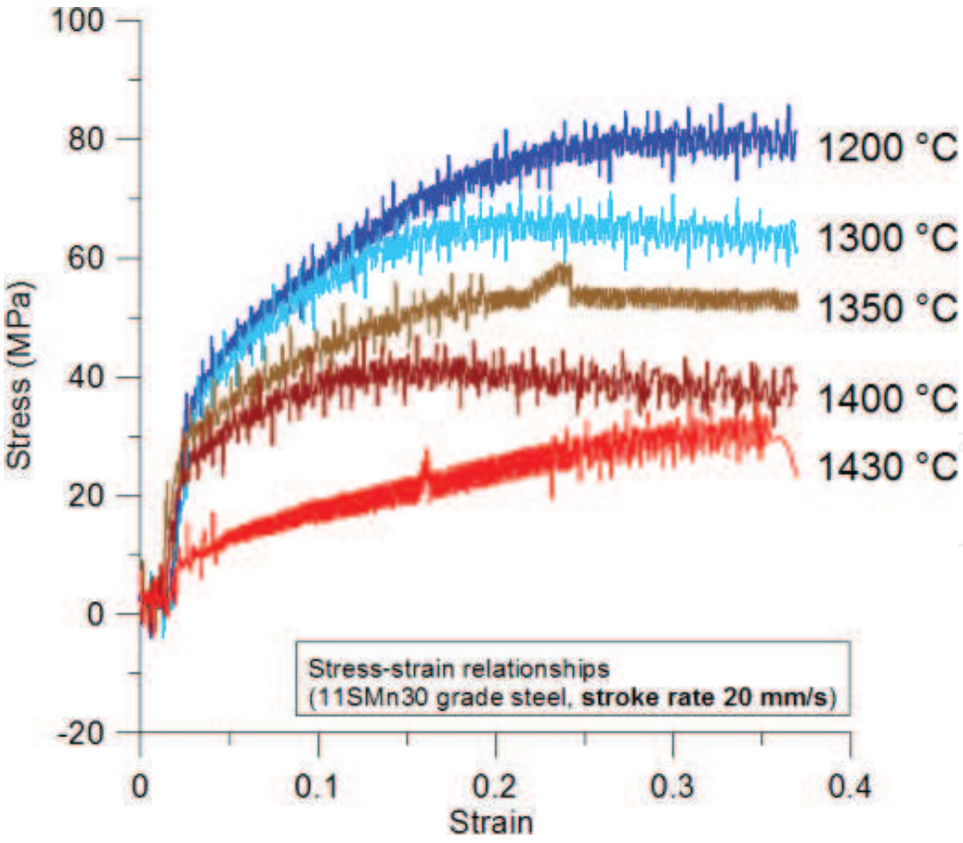

Figure 3. Stress-strain relationships for 11SMn30 grade steel (stroke rate 20 mm/s).

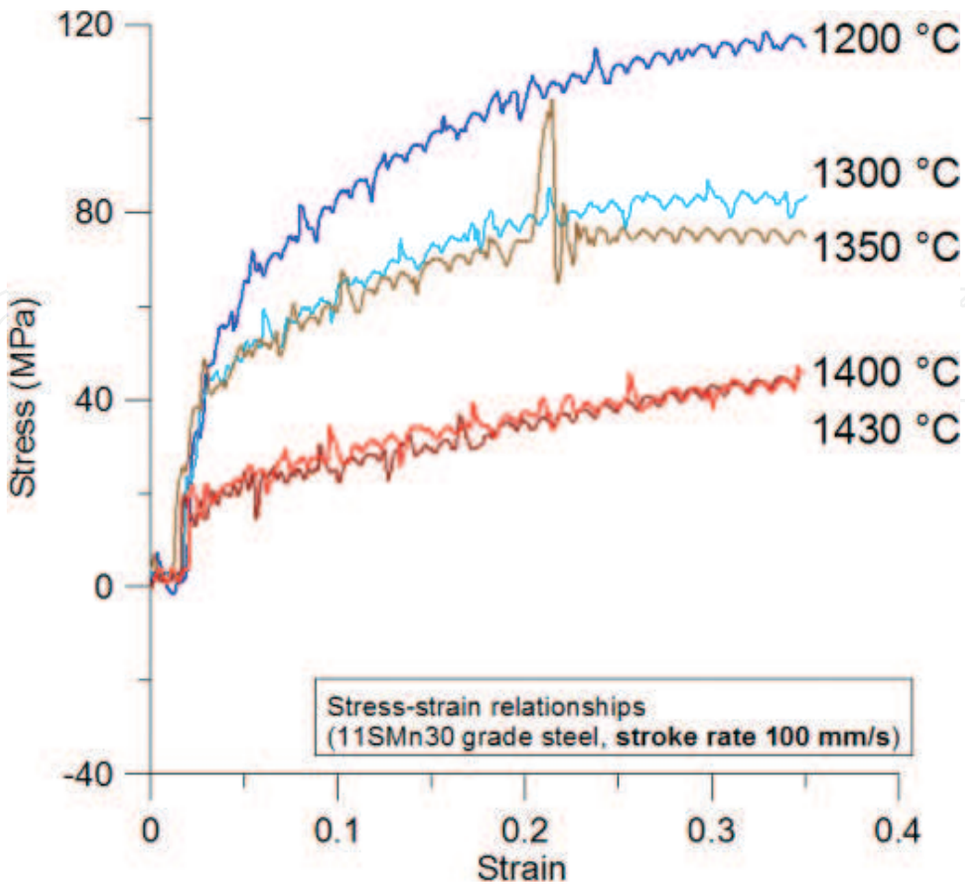

Figure 4. Stress-strain relationships for 11SMn30 grade steel (stroke rate 100 mm/s).

At temperatures a high, even small local temperature variations cause rapid local changes in the stress values. The originally applied NIM methodology supported with inverse calculations, and its later modifications, used axially symmetrical solutions [7]. Comprehensive experimental research carried out as part of the project showed substantial discrepancies between the measured values (e.g. force, temperature) for identically repeated tests. In addition, the developed methodology of a 3D analysis of the sample remelting zone using a modern computer tomograph NANOTOM 180N showed a very high asymmetry of the remelting zones obtained [7], which also proved a high asymmetry of the temperature field within the sample volume. Therefore, the obtained results and the conducted analyses suggested a question whether the use of the NIM methodology—very time consuming and complex in terms of computing—was reasonable. Another relevant aspect was the quality of the developed functions describing changes in stress versus strain, strain rate and temperature. The conducted variant calculations in the first approach using inverse computing and next a new functional model of resistance heating (presented hereinafter) to determine the temperature field after the resistance heating process have led to completely different graphs of stress-strain changes. The mentioned discrepancies, among others, arose from differences in the distribution of the computed temperature field between the two methods, sometimes reaching a few Celsius degrees just in the zone of deformation, and the limitations themselves that arose

http://dx.doi.org/10.5772/67735

from the application of axially symmetrical models. In the light of the above inconveniences, a new methodology DIM (direct identification methodology) was developed. This methodology is presented in detail in the monograph [7]. The DIM utilises data directly recorded by the Gleeble 3800 simulator and the capabilities of the DEFFEM simulation package (**DEFFEM | inverse** module). The new methodology has a great advantage of being fast and flexible in determining function $\sigma_p = f(\varepsilon, \dot{\varepsilon}, T)$ parameters, while maintaining a good compatibility of force parameters between the actual and virtual processes.

In addition, as part of the developed methodology for determining high-temperature characteristics, also macro- and micro-structural tests were performed for each steel tested [7]. Examples of micro-structure of the tested steel 11SMn30 (sample core) deformed at the nominal temperatures of 1350 and 1410°C are presented in **Figure 5**. The analysis of microstructure shows that in the deformation zone acicular ferrite prevails, because of a high deformation temperature and a relatively high cooling rate. The other components of micro-structure are bainite and probably martensite.

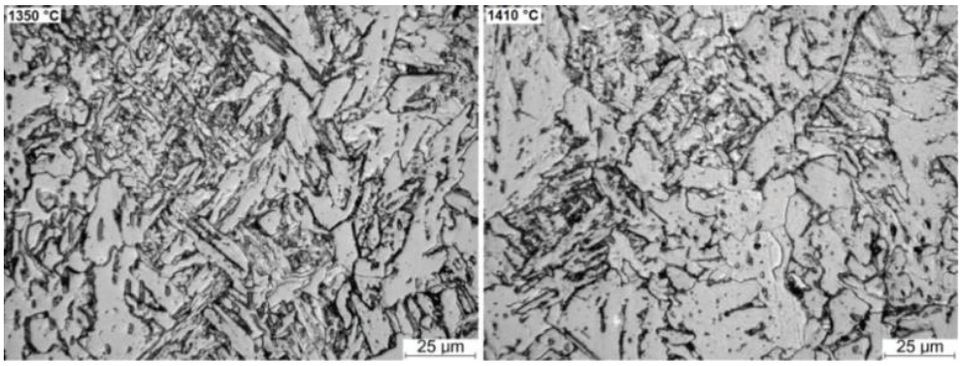

Figure 5. Micro-structure of the core of a sample deformed at a nominal temperature of 1350 and 1410°C (stroke rate 20 mm/s, magnification 400×).

4. Spatial mathematical models

This section presents main assumptions of the implemented 3D models within the DEFFEM package. As mentioned before, two alternative model approaches are developed. The first model approach is the multi-scale model MCFE, which enables heating-remelting, and next deforming in conditions of simultaneous solidification to be simulated. The proposed solution consists of three sub-models: a macro model based on the finite element method providing information about macroscopic behaviour of the medium deformed, a micro-model of the grain-growth process, melting and solidification based upon the Monte Carlo. The last third model is a model that couples the macro- and micro-solutions and facilitates exchange of information between them. The other alternatively developed model approach is a hybrid FESPH model of melting/solidification simulation combining the finite element method (FE) with the smoothed particle hydrodynamics (SPH).

4.1. Multi-scale model

The macro-solution of the mechanical model is based upon the application of a rigid-plastic model for a physical continuum. As showed by tests under conditions of hot deformation, the share of elastic strain in the strain tensor components is small [9, 10]. Applying the law of conservation of energy for a certain isolated system, which in the case concerned is the volume of the metal deformed, one can find that the total work performed in the system in a time unit is equal to the energy that this system gains in the same time. The energy balance for the zone deformed, referred to a time unit may be expressed by the relationship:

$$J = \int_V (\sigma_i \dot{\varepsilon}_i + \lambda \dot{\varepsilon}_{\text{vol}}) dV \tag{2}$$

where σ_i is the effective stress, $\dot{\varepsilon}_i$ is the effective strain rate, $\dot{\varepsilon}_{\text{vol}}$ is the volumetric strain rate and λ is the Lagrange multiplier. Discretisation of the functional (2) is performed in a typical finite element manner using hexahedral elements. The solution in the form of temperature field for the macro-model was searched by solving the Fourier equation, which in the general form can be written as follows:

$$\nabla^T(\lambda \nabla T) + \left(Q - c_p \rho \frac{\partial T}{\partial \tau}\right) = 0 \tag{3}$$

where T is the absolute temperature, λ is the thermal conductivity coefficient, Q is the heat generation rate for volume unit, c_p is the specific heat, ρ is the density and τ is the time.

The thermomechanical solution was directly adapted to the boundary conditions reflecting the Gleeble 3800 thermomechanical simulator system [7]. It allows an easy and fast verification of the obtained simulation results on the basis of experimental data. In classic rigid-plastic solutions, also the term responsible for the power generated as a result of friction on the metal-tool contact should be included in the power functional (2) [9]. Samples in the Gleeble simulator system are fixed in a rigid manner; therefore, the fraction term (coefficient of friction, $\mu = 0$) was not taken into account in the presented model. The resistance heating method is applied for heating of samples in the simulator system. As part of the project, a solution was developed in which a function associating change in the current intensity characteristics over the time, and resistivity versus temperature, was developed. The heat source efficiency Q in the model discussed is a function of resistance R, which in turn depends on temperature T and function A which represents intensify of heating:

$$Q = f\left(A(\tau) I^2(\tau) R(T)\right) \tag{4}$$

It corresponds to resistance changing in the actual model, and the internal heat source efficiency changes together with the resistance. When modelling the Joule heat generation, it was assumed that its equivalent in the numerical model will be the voluminal heat source with its power related to the resistance and the square of electric current I during simulation time τ.

http://dx.doi.org/10.5772/67735

The characteristics of the current intensity change as a function of heating time can be directly recorded during physical tests with the Gleeble 3800 simulator.

The Monte Carlo method was applied to simulate grain growth, melting and solidification. The main idea of the Monte Carlo technique is to divide a solution domain of the material into three-dimensional lattices of cells, where cells have clearly defined interaction rules between each other. Monte Carlo simulations have probabilistic character and base on minimalise system energy. The equation used for grain growth simulations only considers grain boundary energy. The total energy of the system is the total grain boundary energy, which is calculated as the sum of all links between neighbouring cells with dissimilar states multiplied by the link energy as

$$E = J_{gbe} \sum_{<i,\, j>} (1 - \delta_{ij}) \tag{5}$$

where J_{gbe} is the grain boundary energy, i is each cell ranging from 1 to the total numbers of cells, j is the neighbor of site i ranging from 1 to the number of neighbours of i and δ is the Kronecker delta. The kinetics of grain growth is simulated by the selection of a cell and an attempt to change its state and identifier (the number that identifies affiliation to a specific grain) into the state of the neighbouring grain cell. Cells inside a grain, which do not have neighbours belonging to another grain, cannot change their state. When a grain boundary cell attempts to change its state, it selects randomly a state from one of its neighbouring grains. The change energy accompanying this state swap is calculated using Eq. (5) and is accepted with the probability P:

$$P = \begin{cases} e^{-\frac{\Delta E}{kT}} & \Delta E > 0 \\ 1 & \Delta E \leq 0 \end{cases} \tag{6}$$

where kT is the parameter and in the context here and is the simulation temperature. The attempted change in cell state is always successful when $\Delta E \leq 0$. When $\Delta E > 0$, change in cell state is predicted in proportion to the probability P using the Metropolis algorithm [11]. If a randomly generated number R_n from 0 to 1 is less than P, the cell's state is changed into a new one. Otherwise, the cell's state does not change. The very specificity of the heating/remelting process analysed in the Gleeble 3800 simulator system is very similar to the issues related to the welding process and the utilisation of the Monte Carlo method to analyse those processes [11]. **Figure 6** presents macro-structures of samples for two extreme cooling rates (maximum and minimum) and for the rate being their average. Here, we can distinguish four zones: remelting zone (RZ), transition zone (TZ), heat impact zone (HIZ) and grip impact zone (GIZ). The analysis of macro-structures obtained by the experiment and the numerical simulations indicates a large diversification of grain size in individual zones. This arises primarily from various cooling rates achieved locally in individual zones.

The solidification process (without deformation) may be modelled using both the Monte Carlo model and model based on Rappaz-Gandin solutions [7]. The concept of modelling the sample solidification process with its simultaneous deformation required developing an innovative

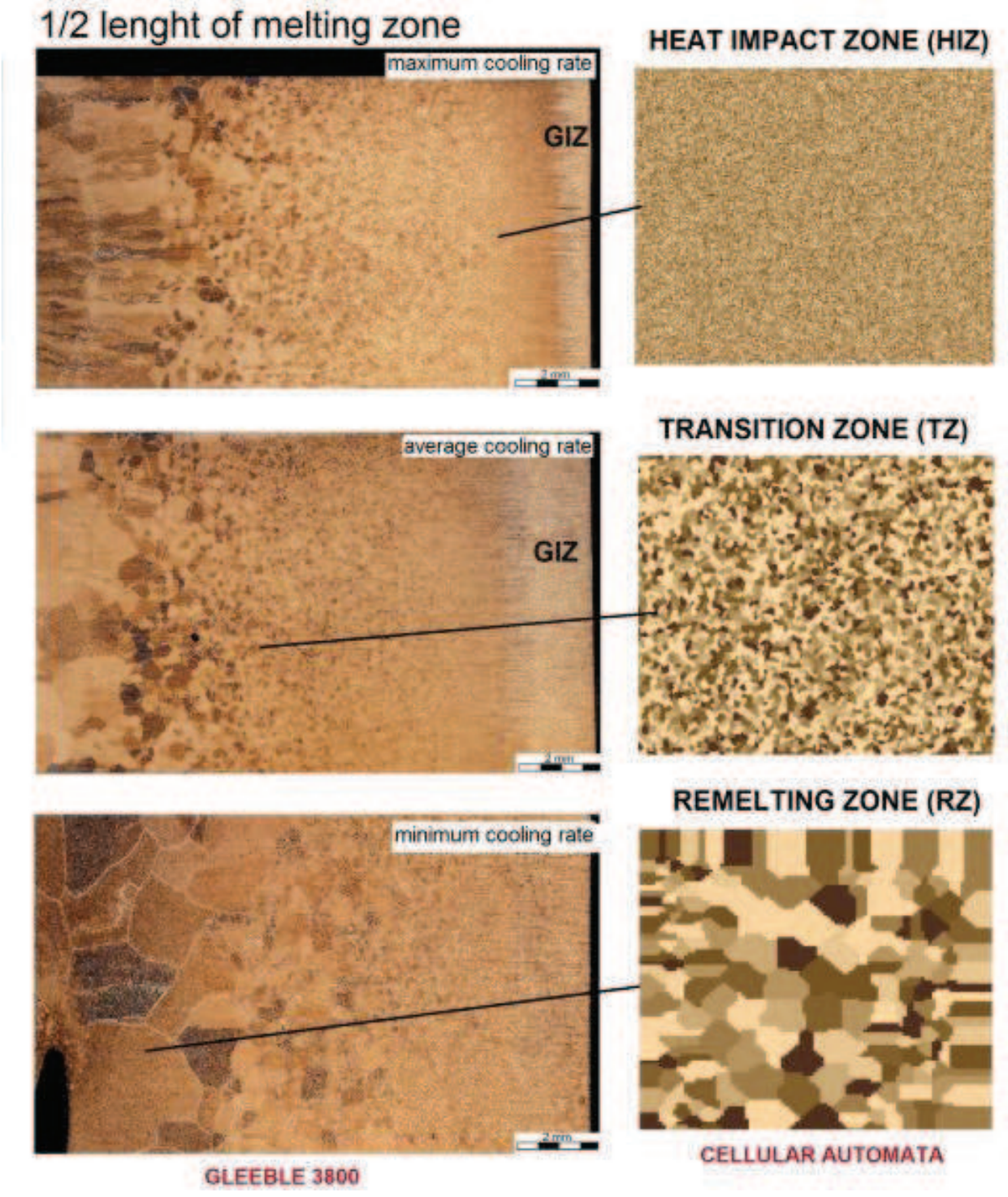

Figure 6. Macro-structure of samples cooled at various rates (physical simulation, computer simulation).

approach to the coupling of the macro-model with the micro-model. The developed MCFE model is based on the assumption that the cells directly correspond to the finite element integration points. As a result, the grain growth, melting and solidification is modelled by the

http://dx.doi.org/10.5772/67735

MC model and deformation process is modelled by the finite element model. A diagram of the macro-(FE) and micro-(MC) model coupling and the information flow is presented in **Figure 7**. Coupling between FE model and MC model is realised by the special Fortran subroutine

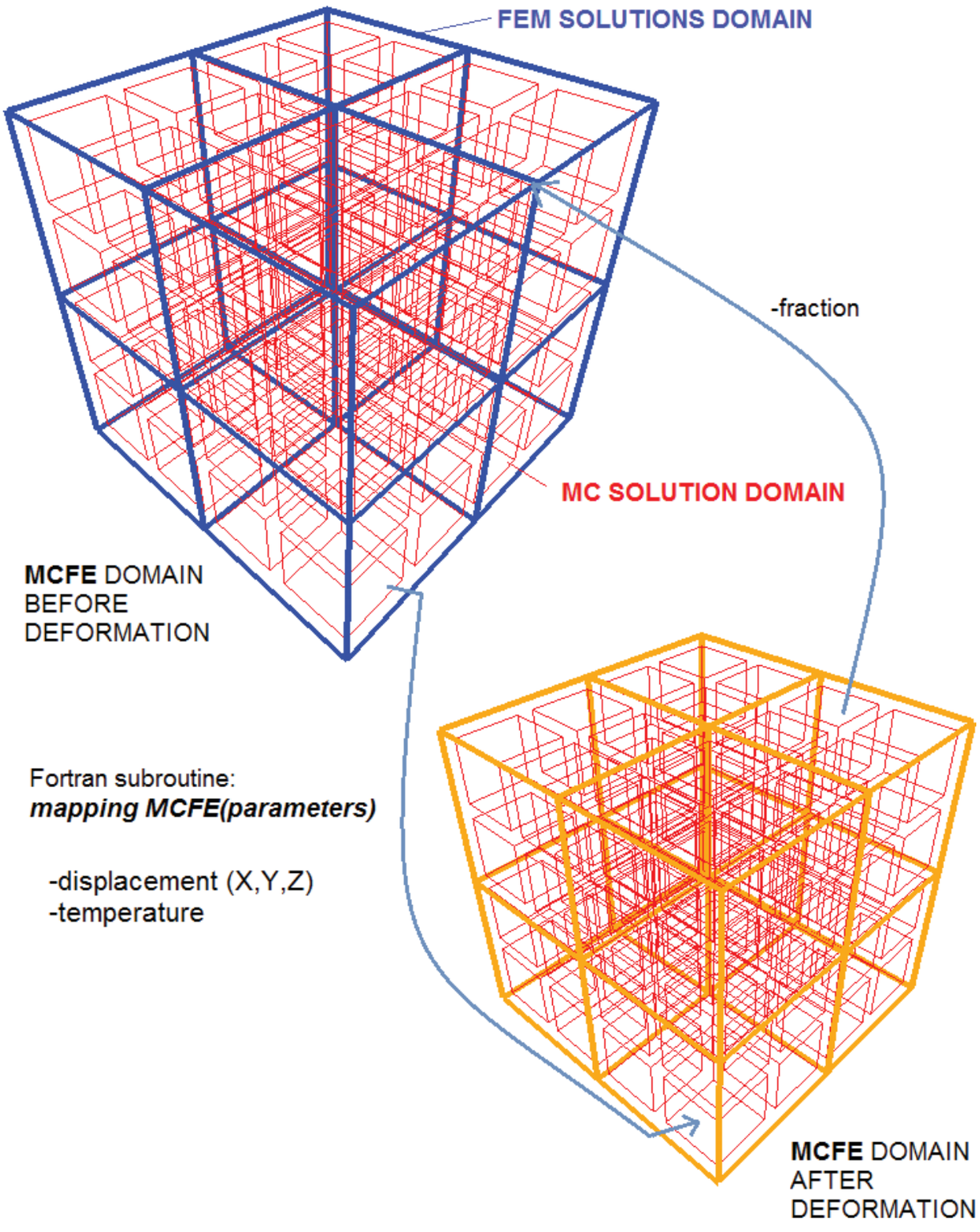

Figure 7. Diagram of the macro (FEM) model and micro (MC) model coupling and the information flow.

mappingMCFE(parameters). In each solution step, information from macro-model regarding positions of integration points and calculated temperatures is send to the micro model. The feedback for the macro-model may be the estimated share of liquid and solid phases which is used to modify the flow stress value for the specified integration point during the next solution step. The whole procedure is performed in a loop to the end of simulation.

4.2. Hybrid model

The hybrid model of the solidification process consists of two solution domains and a special coupling model. The solution of the thermal model based on the finite element method (FEM) is the first solution domain. As part of the first domain, the process of controlled heating/remelting is performed, and next the sample is controlled cooled in the Gleeble 3800 simulator system. The simulation of the solidification process and the liquid steel flow within the solid phase skeleton is performed by the second solution domain based on the smoothed particle hydrodynamics. The governing equations of fluids in the SPH method are based on the Navier-Stokes equations in the Lagrangian form. The main equations are given by [12, 13]

$$\frac{d\rho}{d\tau} = -\rho\nabla \cdot v \tag{7}$$

$$\rho\frac{dv}{d\tau} = -\nabla p + \nabla \cdot \theta + \rho F \tag{8}$$

where τ is the time, v is the velocity, p is the pressure, F is the external force and θ is a second-order tensor containing τ_{ij} stresses. Equation (7) is the continuity equation, which describes the evolution of the fluid density over time, and Eq. (8) is the momentum equation, which describes the acceleration of the fluid medium. By employing the SPH interpolation given by

$$\langle \nabla f(r_i) \rangle \approx \sum_{j=1}^{N} \frac{m_j}{\rho_j} f_j \nabla_i W(r_i - r_j, h) \tag{9}$$

to Eq. (7), the SPH representation of the continuity equation can be written as follow [12, 13]:

$$\frac{d\rho_i}{d\tau} = \sum_{j=1}^{N} m_j (v_i - v_j) \cdot \nabla_i W_{ij} \tag{10}$$

where m_j and ρ_j are the mass and the density for particle j, respectively, W is the smoothing kernel, index j corresponds to any neighbouring particle of particle i, f_j is the value of f for particle j, N is the total number of particles and h is the smoothing length that defines the radius of influence around the current particle i.

The momentum equation can be rewritten in the SPH formalism as

http://dx.doi.org/10.5772/67735

$$\frac{dv_i}{d\tau} = -\sum_{j=1}^{N} m_j \left(\frac{p_j}{\rho_j^2} + \frac{p_i}{\rho_i^2} + \Pi_{ij} \right) \cdot \nabla_i W_{ij} + F \tag{11}$$

The viscous force used in this implementation is the viscosity term which was introduced by Monaghan [12] denoted by Π_{ij}. Equation (11) shows that the change of the motion of a particle is due to the pressure field, the viscosity and the body forces acting on the fluid. An equation of state is required to calculate the pressure in Eq. (11). The equation of state used in the presented model is a quasi-compressible form, which is calculated using the density calculation from Eq. (10) and is given by [12]

$$p = \beta \left[\left(\frac{\rho}{\rho_{\text{ref}}} \right)^{\gamma} - 1 \right] \tag{12}$$

where ρ_{ref} is the reference density, c is the speed of sound, β is the magnitude of pressure, γ=7 for liquid steel. The dynamic particle was selected as a definition of boundary conditions [14].

The model of heat conduction is based on the enthalpy method which is given by [15, 16]

$$\frac{dH}{d\tau} = \frac{1}{\rho} \nabla (\lambda \nabla T) \tag{13}$$

where H is the enthalpy, λ is the thermal conductivity and T is the temperature. The SPH formulation of Eq. (13) is approximated using the SPH which is given by [15]

$$\frac{dH_i}{d\tau} = \sum_j \frac{m_j}{\rho_i \rho_j} \frac{4\lambda_i \lambda_j}{(\lambda_i + \lambda_j)} (T_i - T_j) \frac{(r_i - r_j) \cdot \nabla_i W_{ij}}{(r_i - r_j)^2 + \eta^2} \tag{14}$$

where η is a small parameter to prevent singularity when $(r_i - r_j)$ goes to zero. This equation guarantees that the heat flux is automatically continuous across the different material interfaces, such as between the liquid and solid metals. This also allows multiple phases with different conductivities to be accurately simulated [15]. The model coupling the both domains (FE+SPH) is based upon a solution of coupling by fixing particles to the FE nodes.

5. Computer simulations: example results

This section presents examples of results of numerical simulations performed with the DEFFEM package developed. The first simulation range included the process of heating and deforming within temperature ranges close to the solidus line (without the liquid phase). The obtained findings were verified on the basis of the developed methodology of deformation zone measurement using 3D scanning technology with blue light [7]. The second stage of work included simulations concerning fluid mechanics. The obtained findings were verified on the basis of well-known laws of physics.

5.1. Test simulations of the DEFFEM|solver_3D_TM

The numerical simulations and experiments were carried out with two types of hexahedral samples with a cross-section 10 × 10 mm and lengths of 100 mm (sample type B) and 125 mm (sample type C) made of steel S355 [7, 17]. The experiments and numerical computations were conducted on the basis of the research methodology presented in study [7]. In the simulation, a sample was heated to a temperature of 1400°C at a rate of 20°C/s, and next to a temperature of 1450°C at a rate of 1°C/s. **Figures 8–11** present the temperature distribution for the selected heating stages for both sample types. Referring to the observed temperatures at the sample surface and the maximum temperatures achieved in the sample core, one may observe an increasing temperature gradient on its cross-section as the heating time passes. For a sample type B, after 10 s this difference was 4.4°C, after 70 s growing up to 33.9°C. For the variant with a sample type C (longer), these differences were slightly bigger and were 4.7 and 35.2°C, respectively.

In order to verify the obtained results of the heating simulation in the experiments, a thermovision camera was used to record the profile of the temperature change along the sample heating zone (**Figure 12**).The obtained results of the experiment and simulation are characterised by a parabolic course, and the correct compatibility between the experimental and calculated values. The average relative error calculated for 13 checkpoints was 14.5%. At the last stage, the deformation process was performed, assuming the stroke of 5 mm and the stroke rate of 1 mm, following sample cooling at a rate of 10°C/s to the nominal deformation temperature. The deformation experiments were performed for a temperature scope 1200–1400°C. **Figure 13** presents the total Z displacement distribution and the general characteristics of boundary conditions identified in the Gleeble simulator system and adapted to the numerical solution [7]. Three main zones can be distinguished for both sample types. The first zone (sample fixed) defines the grip contact area that does not move during the physical simulation

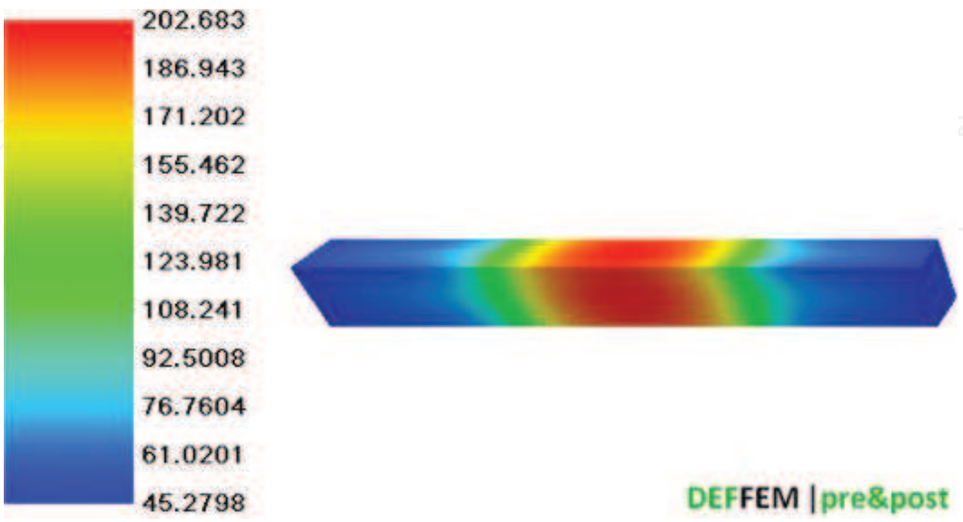

Figure 8. Temperature distribution after 10 s of heating (sample type B, surface temperature 198.286°C).

http://dx.doi.org/10.5772/67735

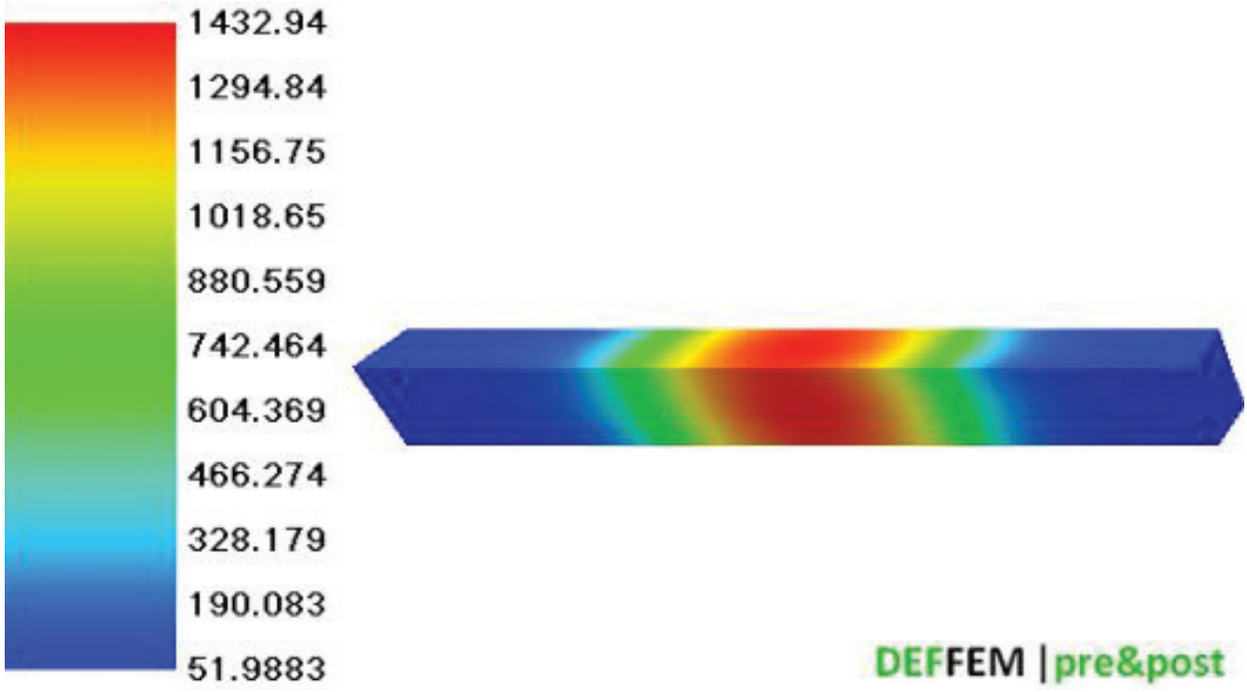

Figure 9. Temperature distribution after 70 s of heating (sample type B, surface temperature 1.399.13°C).

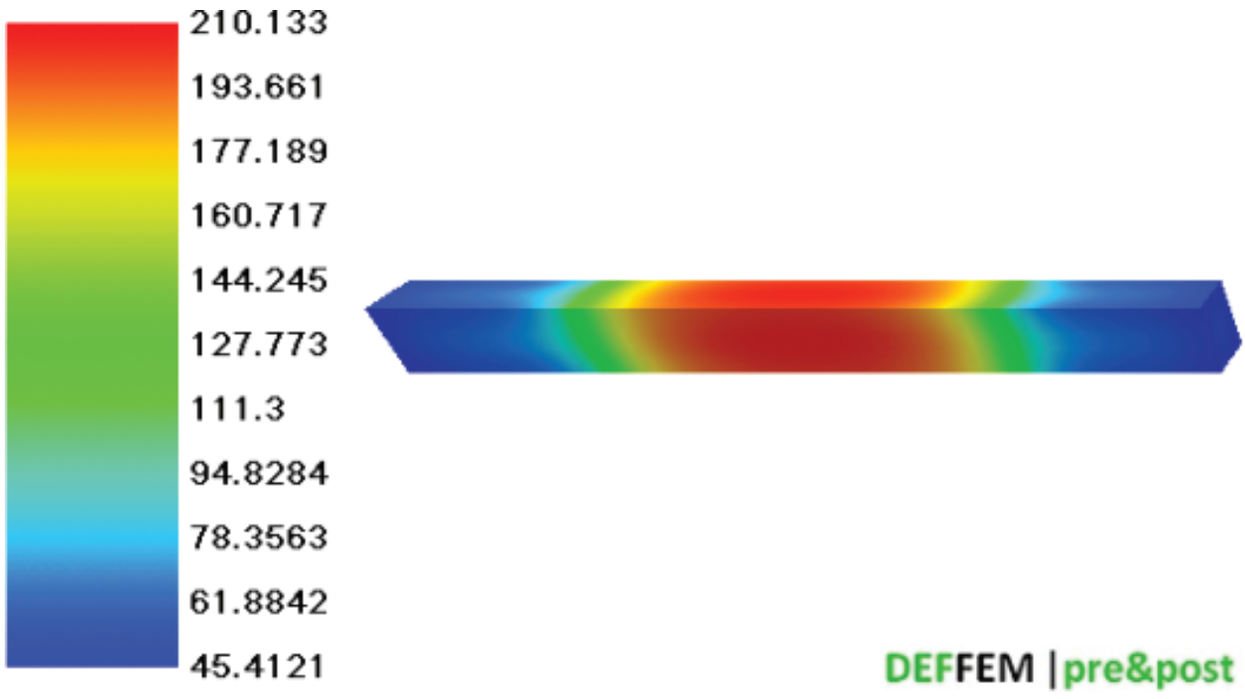

Figure 10. Temperature distribution after 10 s of heating (sample type C, surface temperature 205.405°C).

and the second zone (sample movement) is the grip contact zone that moves by a set stroke. The central zone is a free zone with the highest strain accumulation, which for a sample type B is 39.5 mm long.

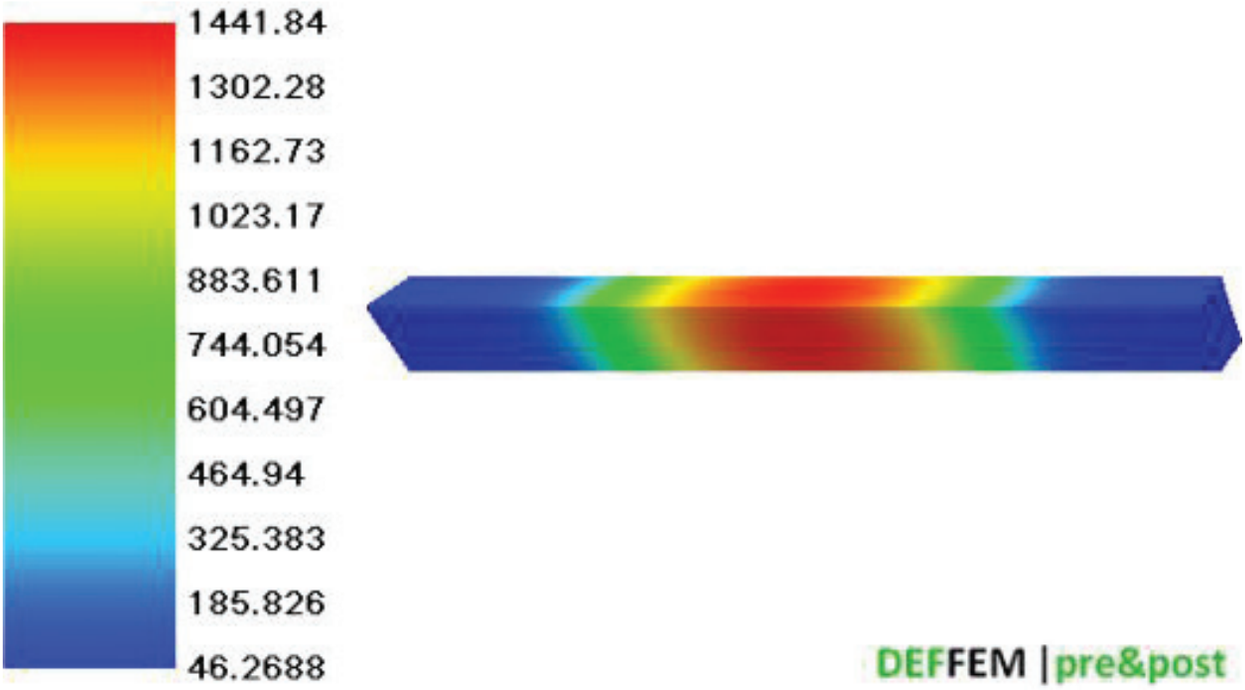

Figure 11. Temperature distribution after 70 s of heating (sample type C, surface temperature 1.406.63°C).

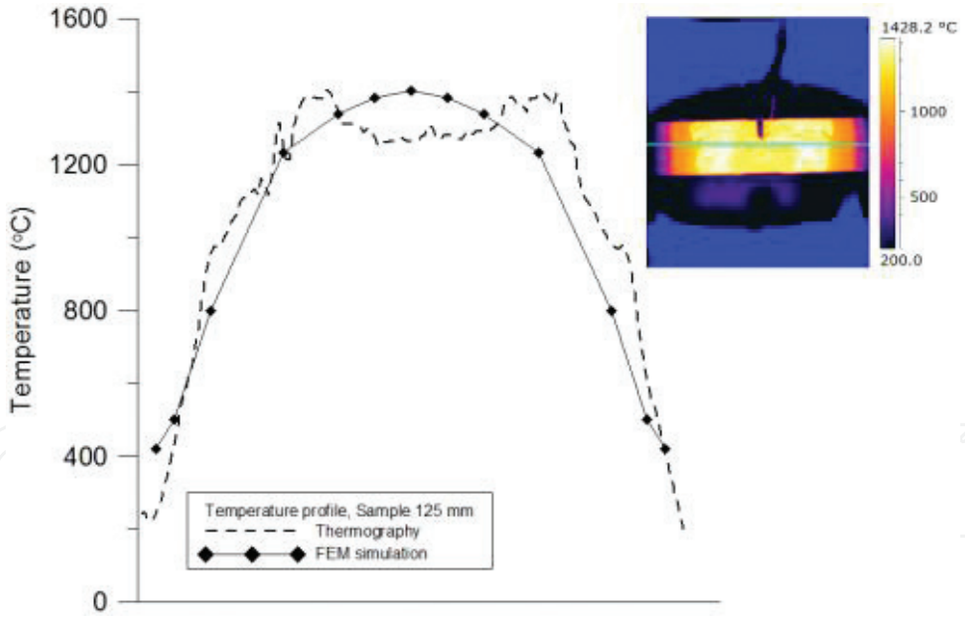

Figure 12. The temperature profile along the heating zone calculated and determined by the experiment (test nominal temperature 1400°C, sample type C).

Figures 14 and **15** present the strain distribution (ε_z component) for the strain variant at two nominal temperatures 1200 and 1400°C. Strain cumulates mainly in the central deformation zone, reaching slightly higher values for the deformation test performed at a temperature of 1400°C.

http://dx.doi.org/10.5772/67735

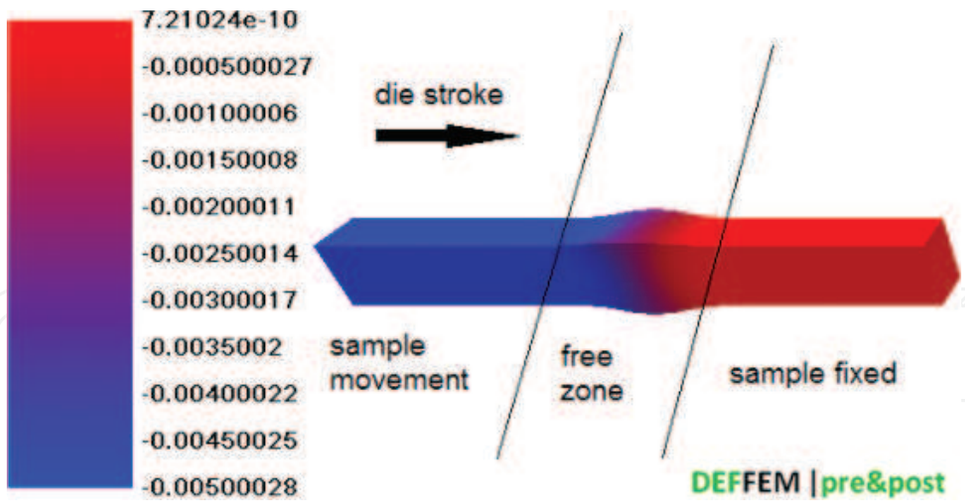

Figure 13. Total Z displacement distribution (sample type B, test nominal temperature 1400°C).

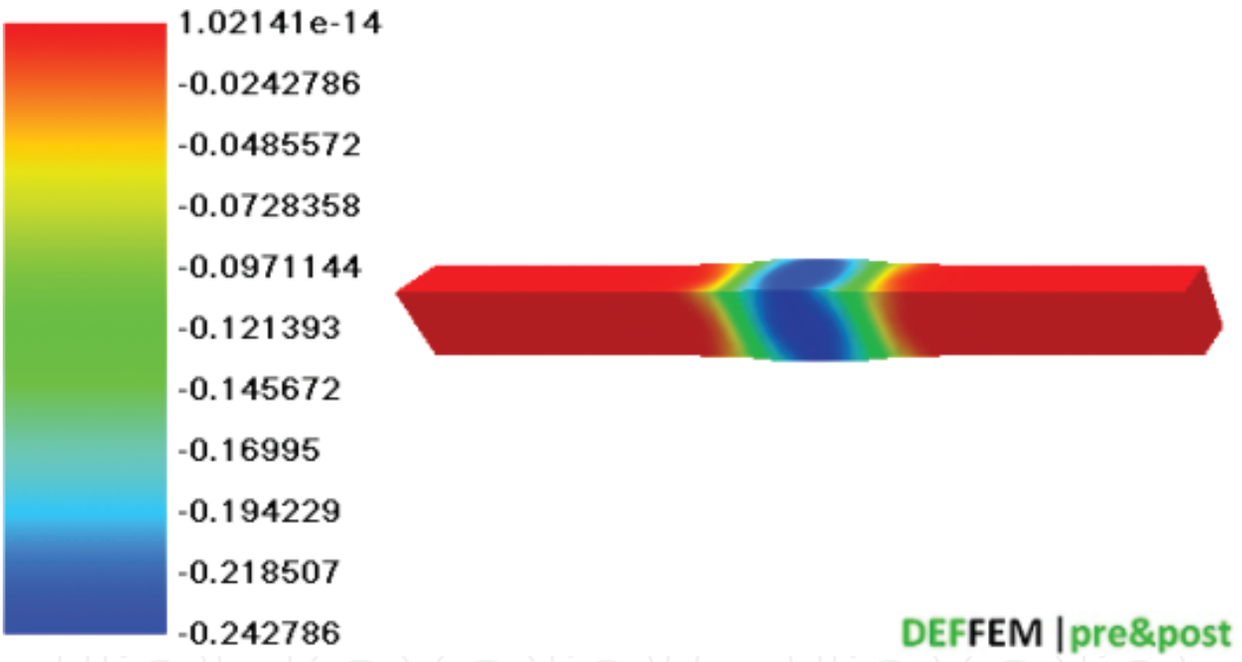

Figure 14. Strain distribution, ε_z component (sample type C, test nominal temperature 1200°C).

Analysing the shape and size of the strain zones resulting from the simulation (**Figures 14** and **15**) and experiment (**Figure 16**), one may observe that they feature a very high geometrical similarity. To verify the obtained findings, the developed measurement methodology with blue light scanning was applied [7]. **Figure 17** presents a map of deviations between the obtained numerical calculation meshes after the deformation process at a temperature of 1200 and 1400°C. The sample deformed at 1200°C was selected as the standard in the mapping procedure. The analysis of the obtained results indicates an increase in the cross-section of the sample deformed at 1400°C, and a slight decrease in the strain zone length compared to the sample deformed at 1200°C.

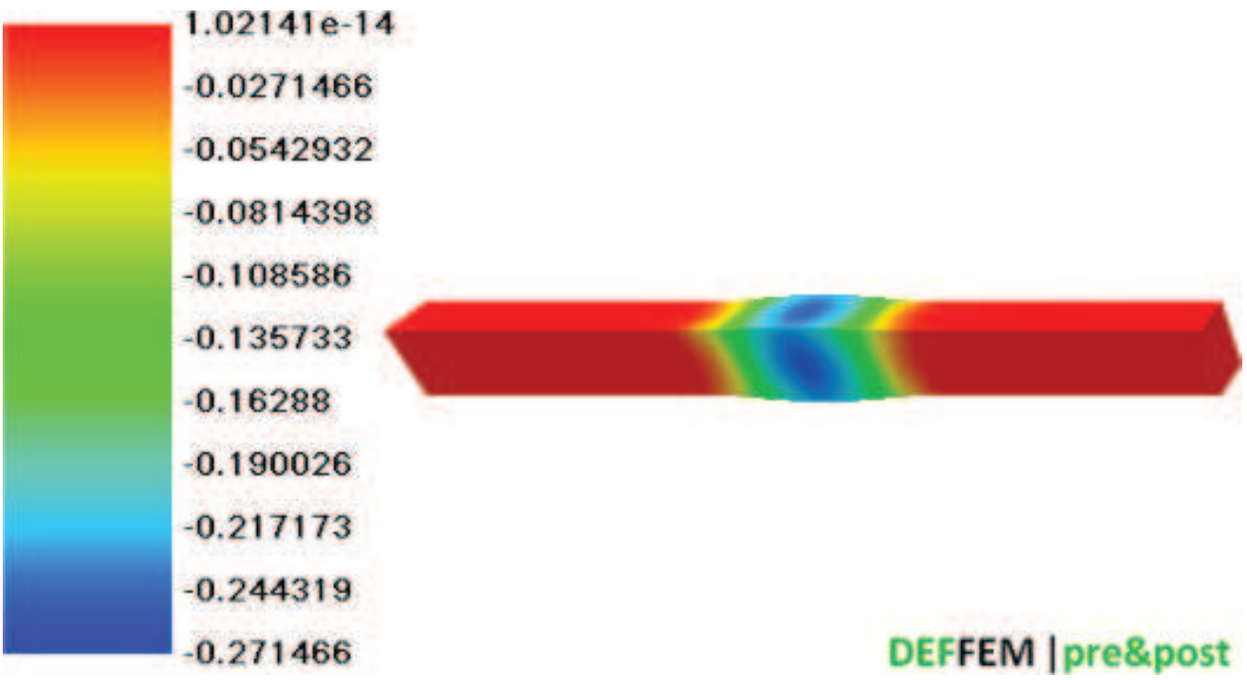

Figure 15. Strain distribution, ε_z component (sample type C, test nominal temperature 1400°C).

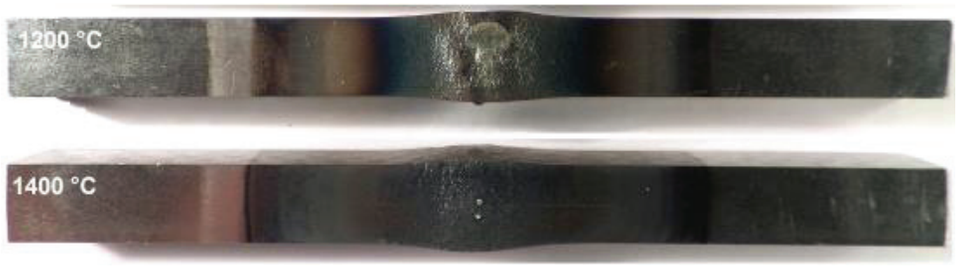

Figure 16. Pictures of samples after deforming at 1200 and 1400°C (sample type C).

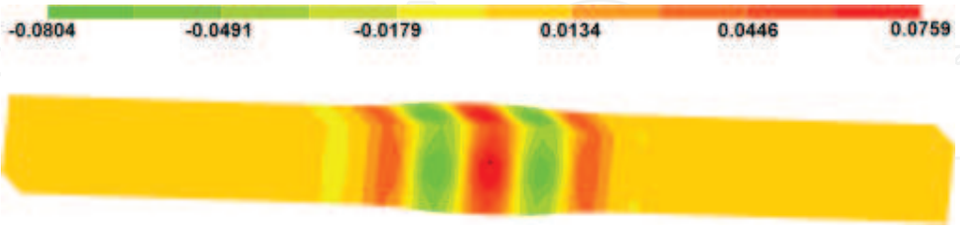

Figure 17. The deviation map between two finite element meshes for two deformation temperatures (sample type C).

An analogous methodology was applied to compare the obtained shape of the deformation zone from the computer simulation to the experimental shape (**Figures 18–25**). An analysis of the obtained deviation maps indicates that the local difference of 1 mm was not exceeded in any case. The maximum absolute value was 0.99 mm for a sample type B deformed at a temperature of 1400°C and the minimum absolute value of 0.4583 mm for a sample type B deformed at 1350°C.

http://dx.doi.org/10.5772/67735

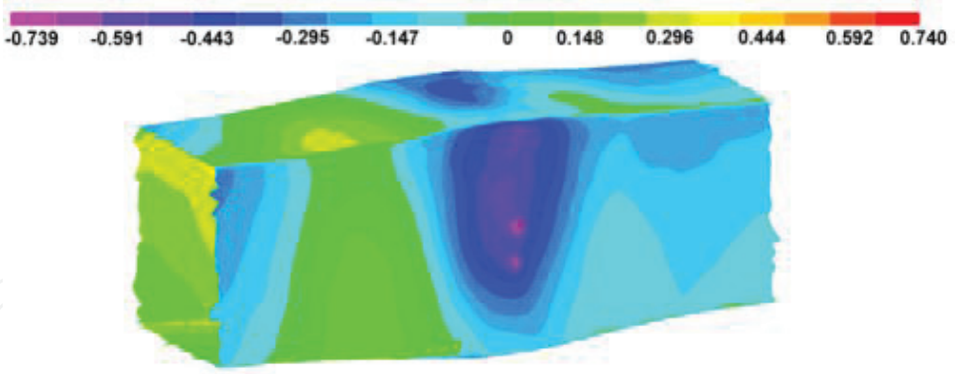

Figure 18. The deviation map between the finite element mesh and the mesh obtained from the 3D scanner (sample type C, 1200°C).

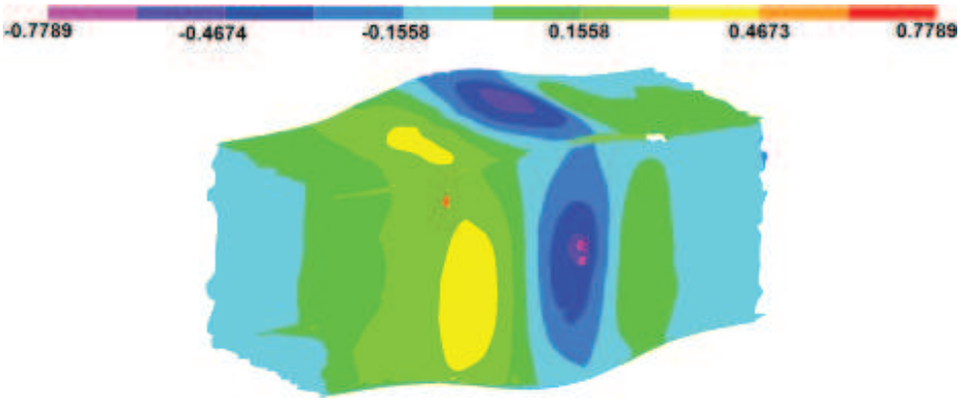

Figure 19. The deviation map between the finite element mesh and the mesh obtained from the 3D scanner (sample type B, 1200°C).

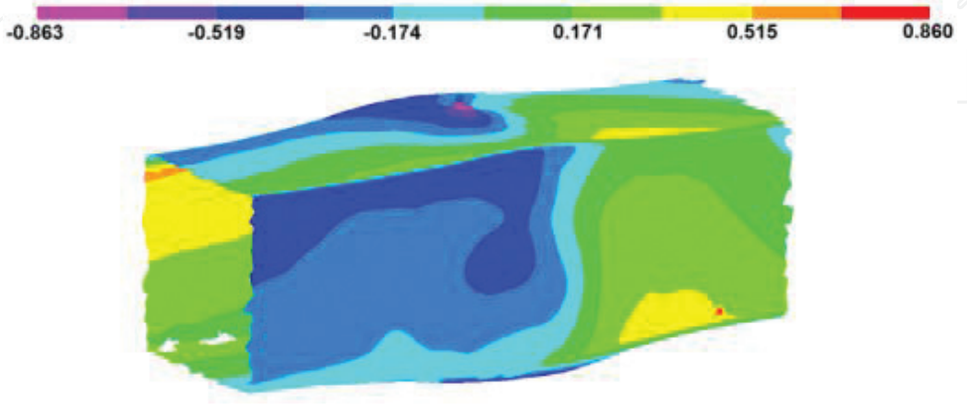

Figure 20. The deviation map between the finite element mesh and the mesh obtained from the 3D scanner (sample type C, 1300°C).

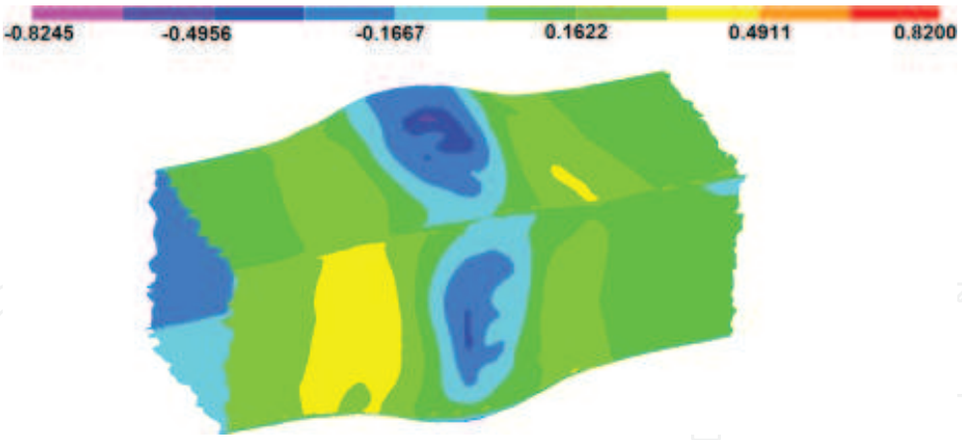

Figure 21. The deviation map between the finite element mesh and the mesh obtained from the 3D scanner (sample type B, 1300°C).

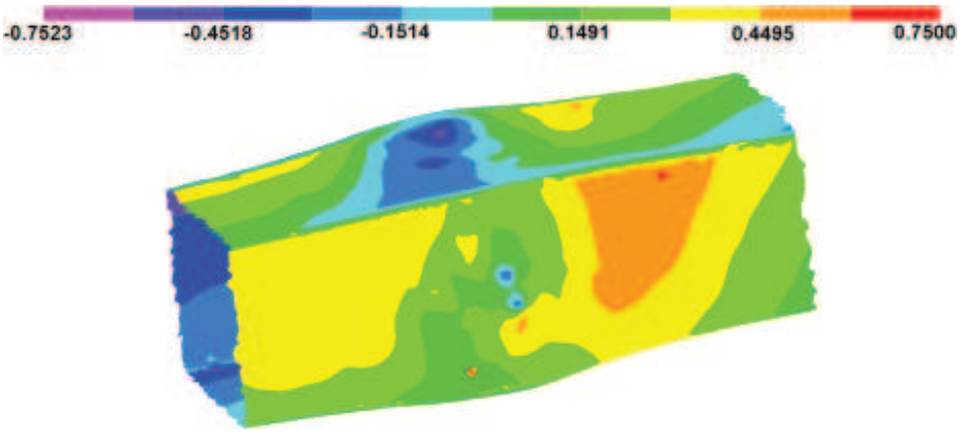

Figure 22. The deviation map between the finite element mesh and the mesh obtained from the 3D scanner (sample type C, 1350°C).

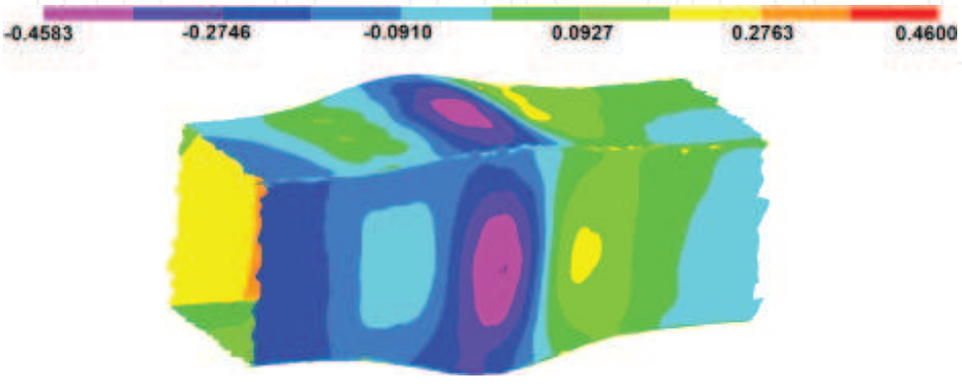

Figure 23. The deviation map between the finite element mesh and the mesh obtained from the 3D scanner (sample type B, 1350°C).

http://dx.doi.org/10.5772/67735

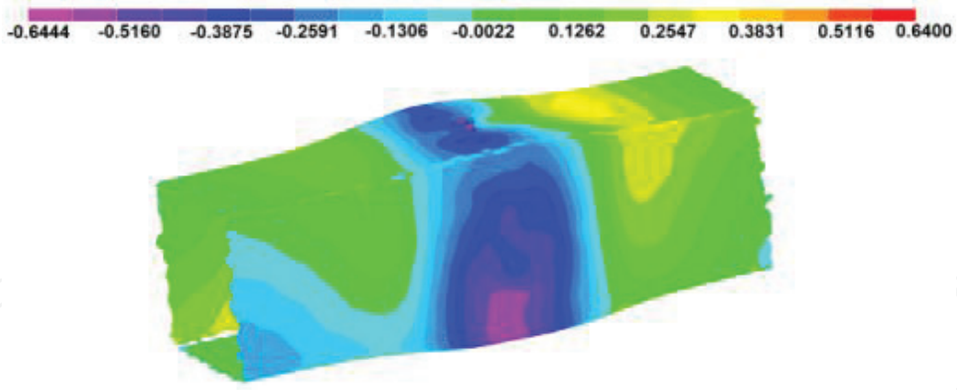

Figure 24. The deviation map between the finite element mesh and the mesh obtained from the 3D scanner (sample type C, 1400°C).

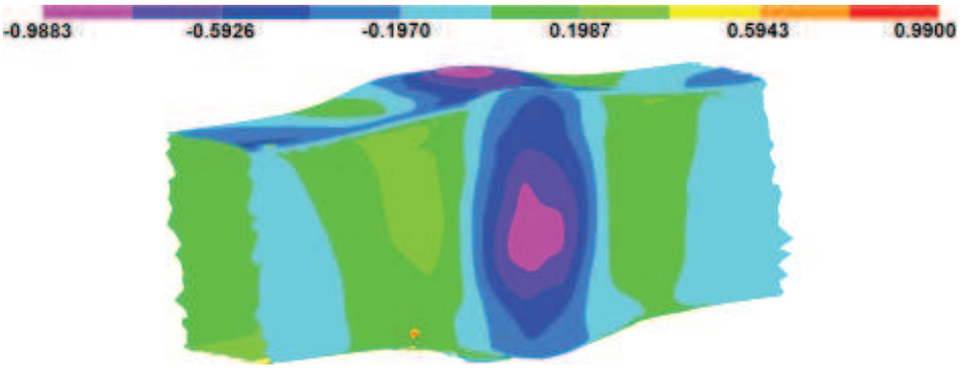

Figure 25. The deviation map between the finite element mesh and the mesh obtained from the 3D scanner (sample type B, 1400°C).

5.2. Test simulations of the DEFFEM|solver_3D_FLUID

Two simulations were carried out as part of the test simulations of the fluid mechanics solver. The first case of free particles fall was carried out in order to check the Runge-Kutta integration scheme used in the implementation. The second one is oriented for a structure impact simulation based on dynamic particles. The main feedback from this case is: can the dynamic particles handle this kind of boundary condition. The schemes of initial geometries of these problems are presented in **Figures 26** and **27**. Solution domain consists of 7351 (free fall case)/29,791 (barrier case) moving particles and 29,402 (free fall case)/34,443 (barrier case) dynamic particles represents boundary condition as a box given from particle to particle (width = 1.0 m, height = 1.0 m and length = 1.0 m). The initial drop height for free fall case was set 0.3 m. Other parameters adopted as: initial smoothing length= 0.024 m, speed of sound 30 m/s, α is equal to 0.5 and simulation time: 2.0 s.

Figure 28 presents the velocity field for a simulation time of 0.2 s, where the solution domain (fluid) did not interact with the substrate defined by dynamic particles representing the boundary condition. The mean particle velocity is around a given value 2 m/s. The current velocity perfectly corresponds to what is expected by the analytical solution (~1.96 m/s). On

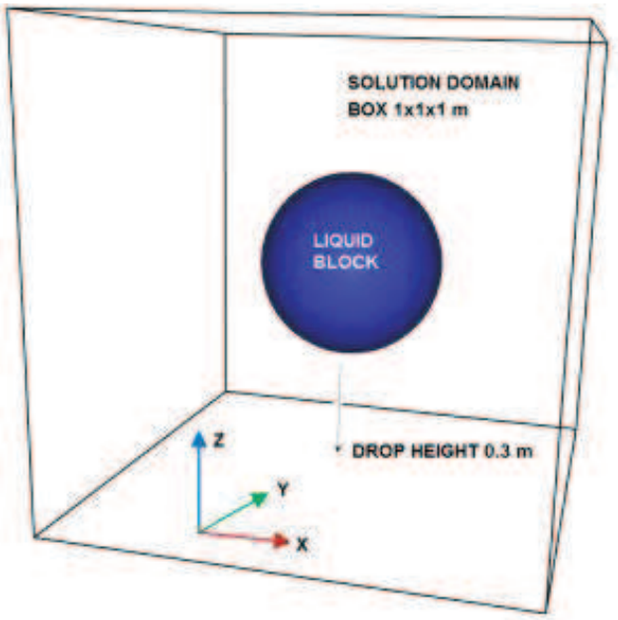

Figure 26. Solution domains for the 'free fall' test simulation.

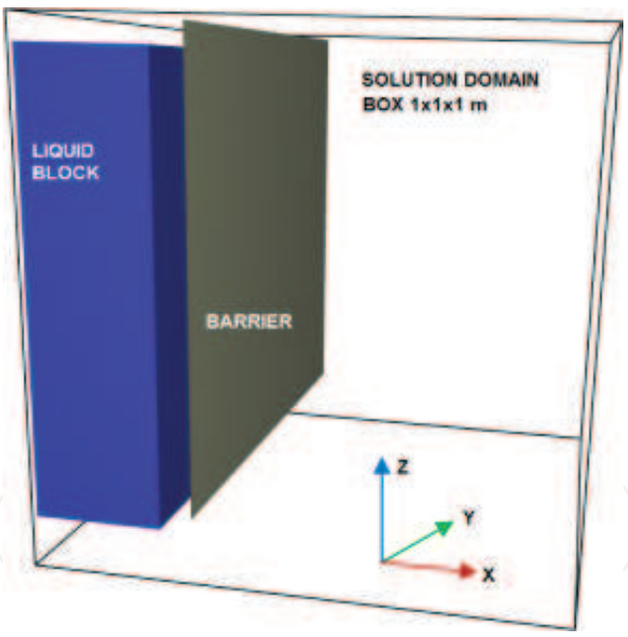

Figure 27. Solution domains for the 'barrier' test simulation.

the other hand, **Figure 29** presents the velocity field for a simulation time of 1.96 s, where the velocity field has already stabilised.

Analytical solutions and numerical solutions of a particle fall in respect to z position correspond excellent to what is expected by the analytical solution. Starting z position of particle ID:1 = 0.44 m, calculated z position of particle ID:1 = 0.24372551083597468 m after 0.2 s. Analytical solution z position of particle ID:1= 0.243718462 m after 0.2 s. This result indicates

http://dx.doi.org/10.5772/67735

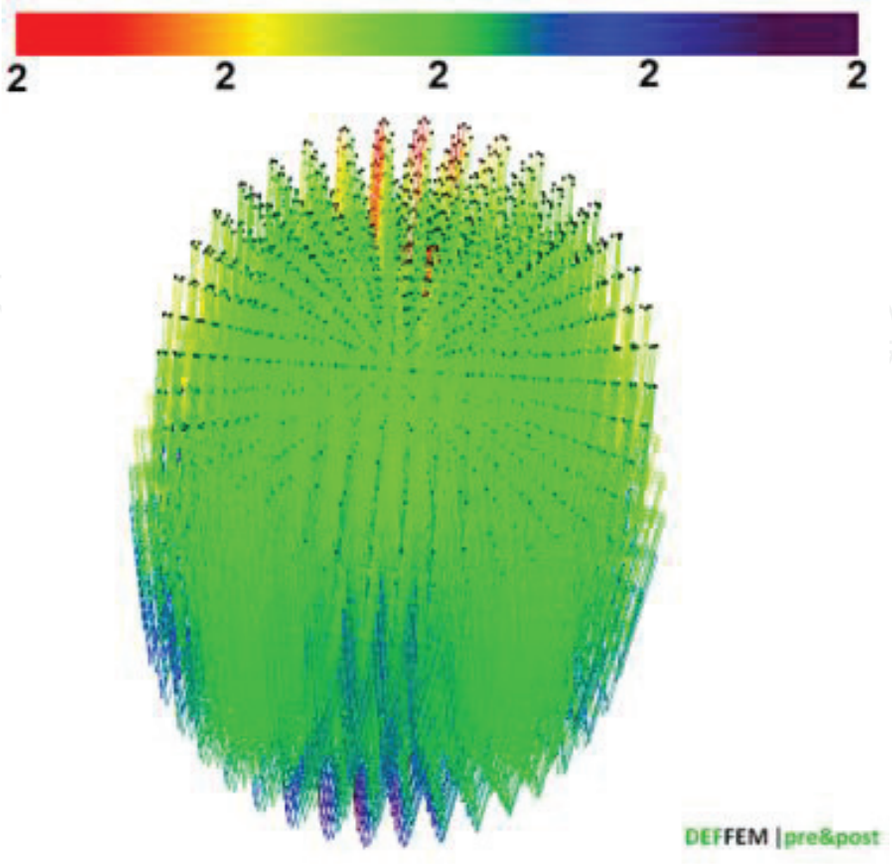

Figure 28. Vector velocity field (simulation time 0.20004155454510358 s).

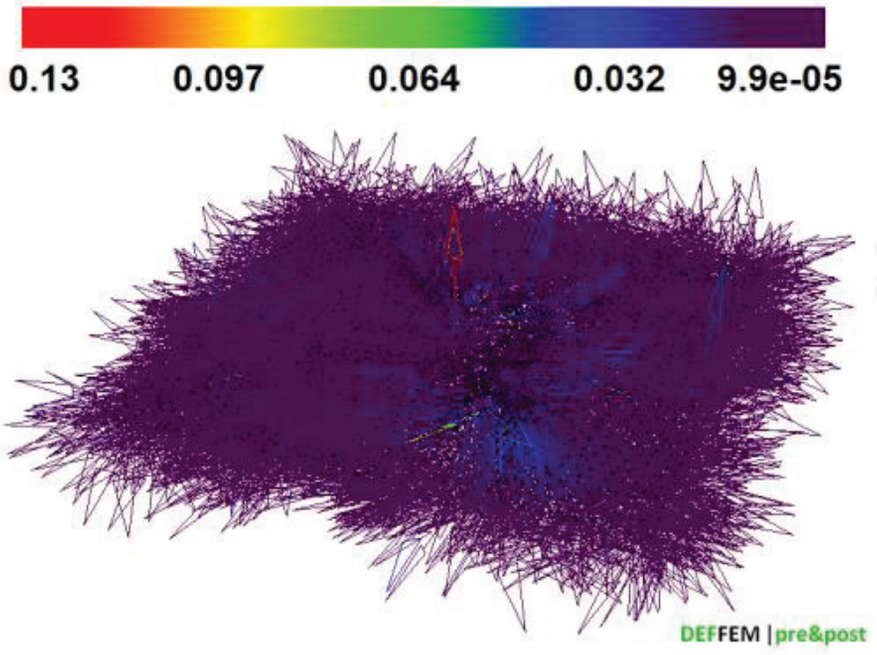

Figure 29. Vector velocity field (simulation time 1.9600608766537435 s).

that the Runge-Kutta integration scheme used in the implementation works correctly. **Figures 30–35** present the selected stages of the free flow simulation taking account of the fluid-structure interaction. The analysis of the obtained results indicates that the implemented

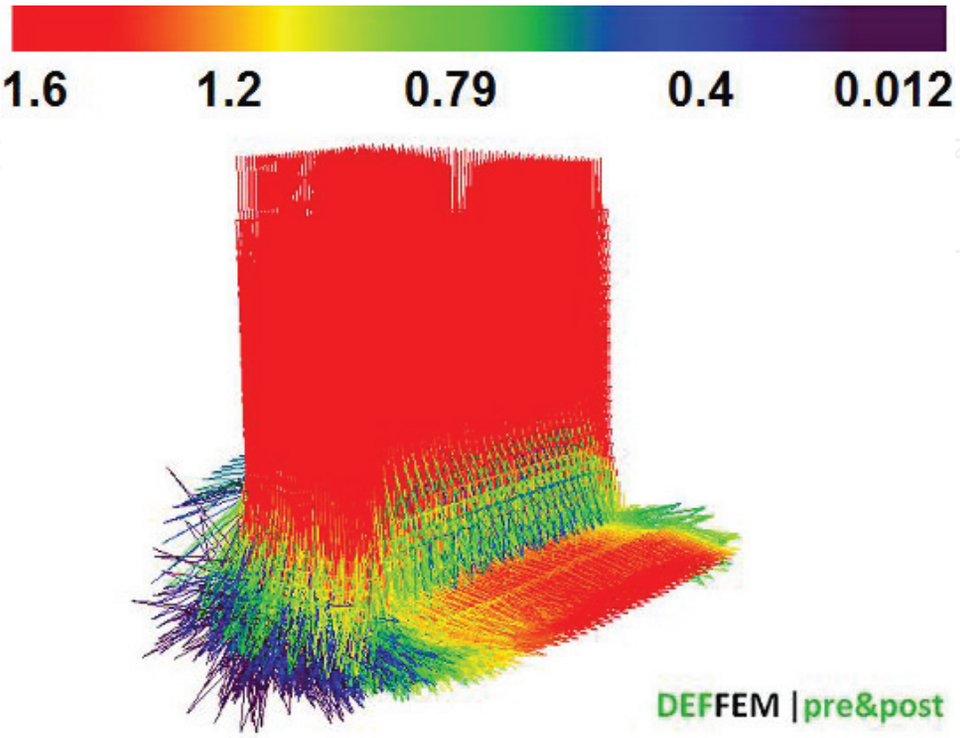

Figure 30. Vector velocity field (simulation time 0.16001791210049551 s).

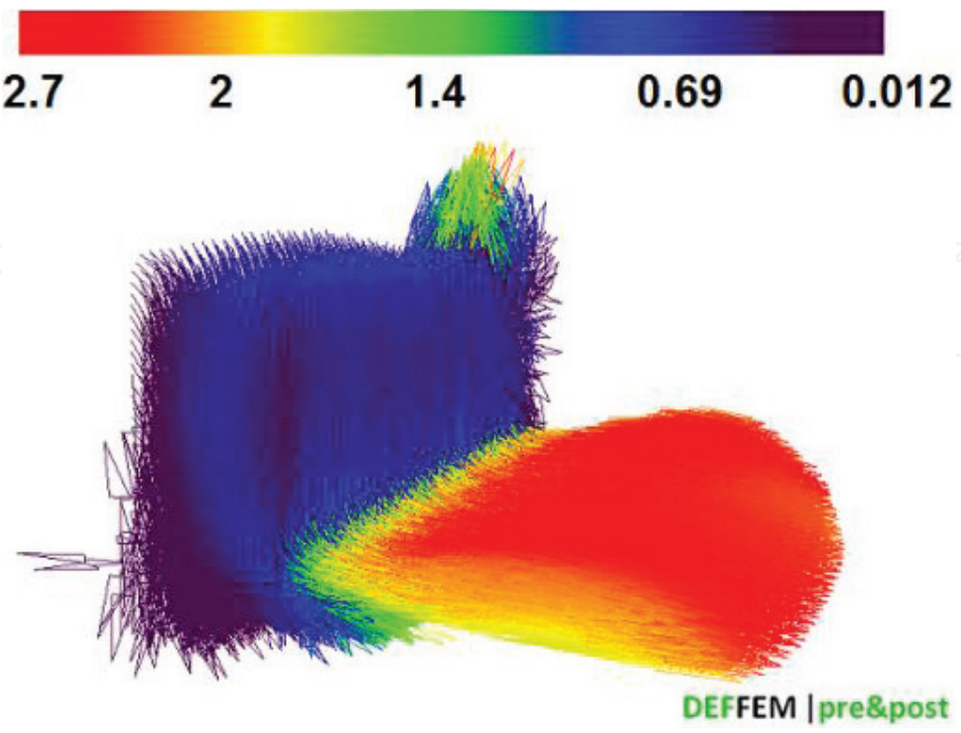

Figure 31. Vector velocity field (simulation time 0.36004176147624667 s).

http://dx.doi.org/10.5772/67735

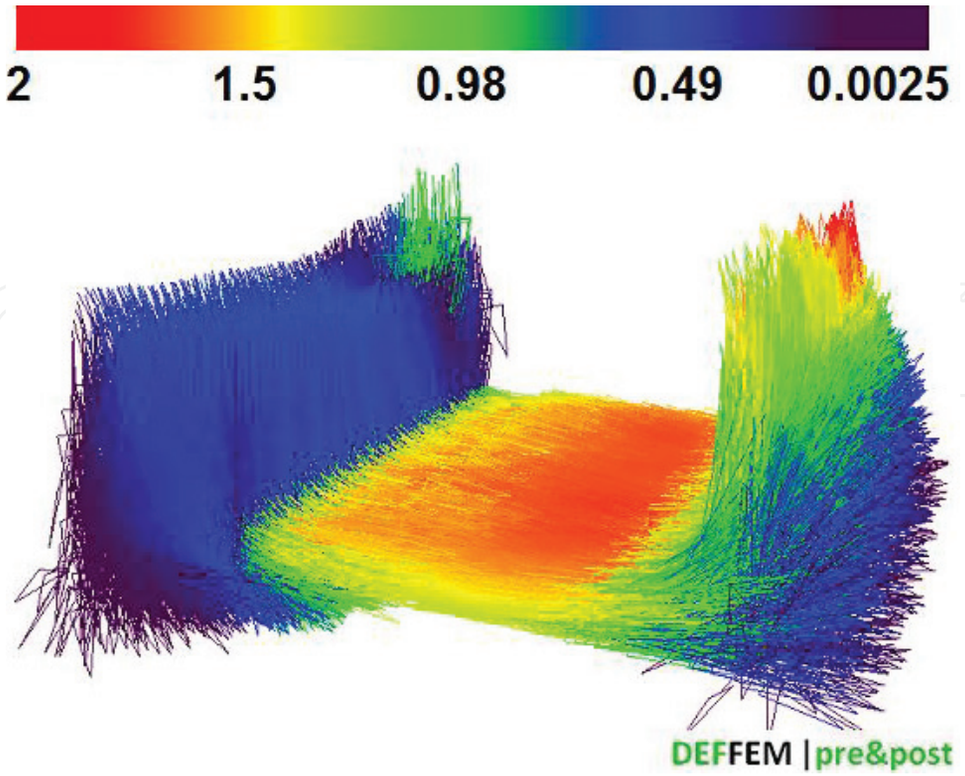

Figure 32. Vector velocity field (simulation time 0.56007371089547675 s).

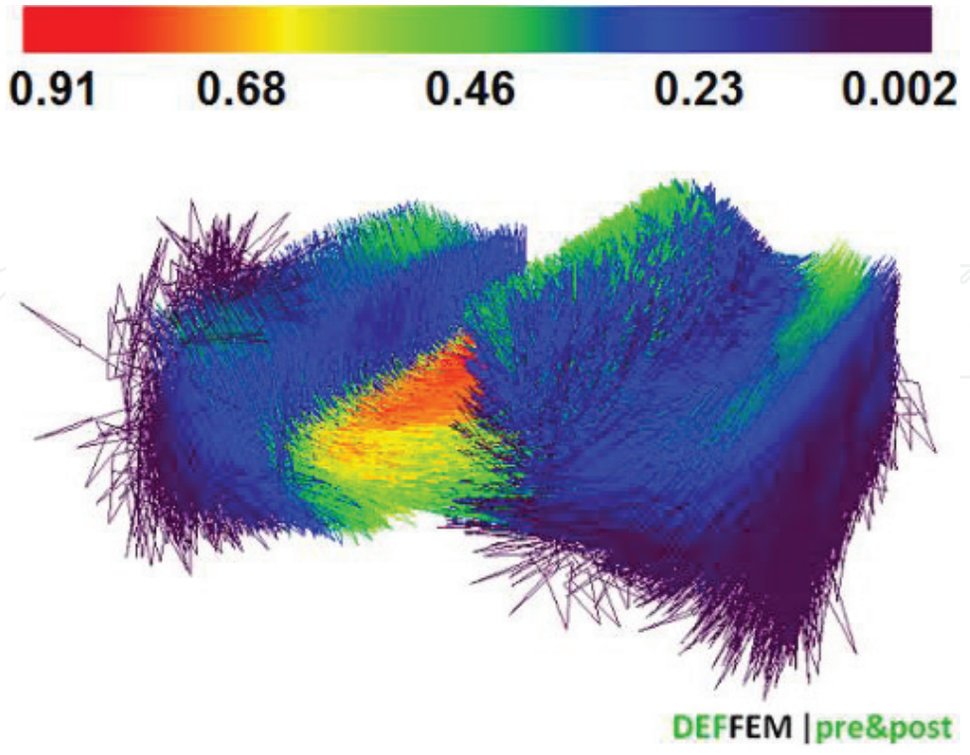

Figure 33. Vector velocity field (simulation time 0.96000801664997626 s).

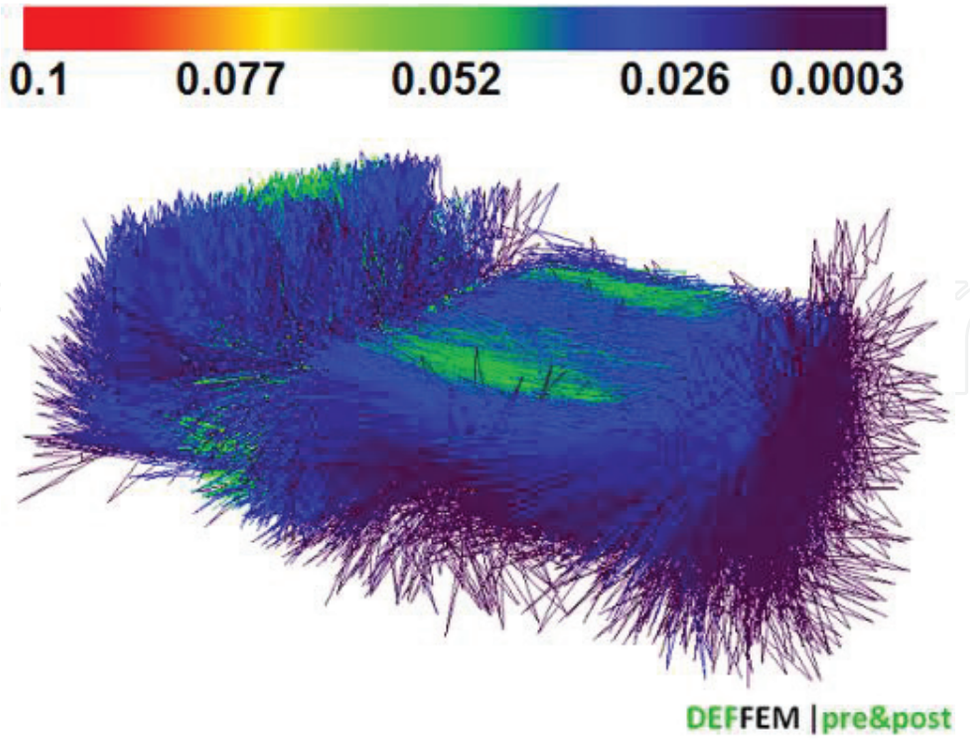

Figure 34. Vector velocity field (simulation time 1.5600837463861228 s).

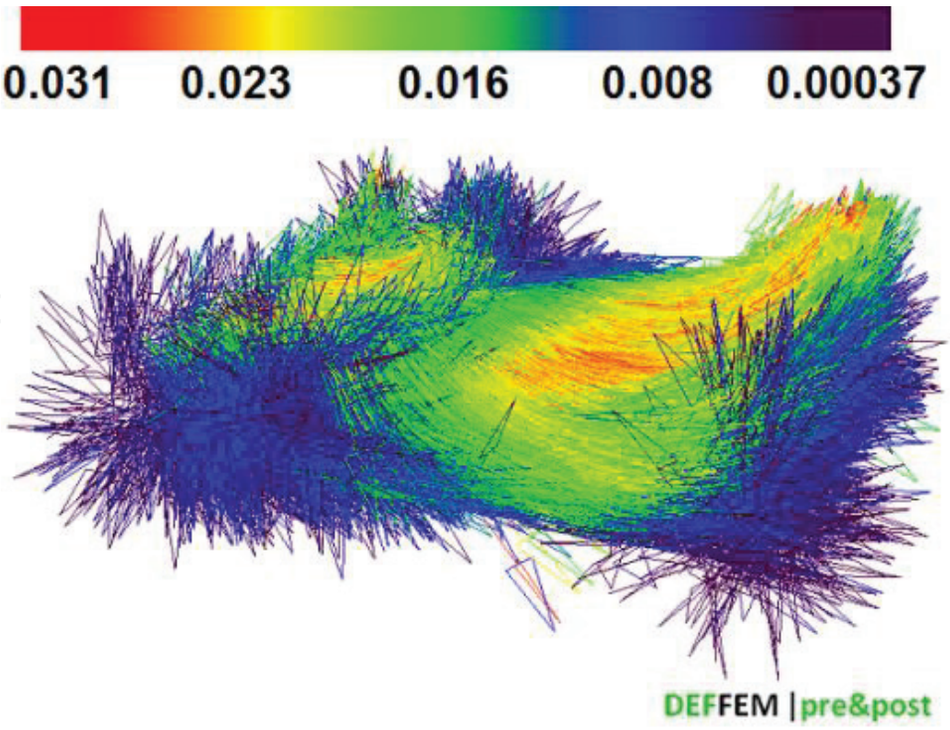

Figure 35. Vector velocity field (simulation time 2.0000482073234136 s).

http://dx.doi.org/10.5772/67735

interaction model is correct. We can observe a greater speed when the fluid passes through the barrier defined by dynamic particles. The velocity is increased as a high repulsion force is created by the boundary defined by dynamic particles (**Figure 31**). In the subsequent steps of the simulation, the fluid in the computing domain slowly equalises and the velocity field slowly stabilises (**Figures 34** and **35**). However, more tests for various variants are required for further detailed verification.

6. Summary

This chapter presents a multi-scale model MCFE (Monte Carlo and finite element) and a hybrid model FESPH combining the advantages of the finite element method (FEM) and the smoothed particle hydrodynamics (SPH). The developed models and methods constitute the basis of the scientific workshop focused on high-temperature processes. A great advantage of a solution like this is the full openness of source codes of the simulation system designed, which will be the basis for developing further new and innovative solutions. The conducted test simulations concerning continuum mechanics (the FEM solution) and fluid mechanics (the SPH solution) indicate the correctness of the implemented mathematical models in the context of determining temperature fields, strains or velocity fields. The DEFFEM package was successfully applied in practical projects accomplished with industrial partners as a design aiding tool. The present tests in collaboration with an industrial plant from the aviation and casting industry will allow us to perform additional industrial tests and to evaluate the suitability of the software in the computer-aided design.

Acknowledgements

The research has been supported by the Polish National Science Centre (2012–2017), decision number: DEC-2011/03/D/ST8/04041.

Author details

Marcin Hojny

Address all correspondence to: mhojny@metal.agh.edu.pl

AGH University of Science and Technology, Kraków, Poland

References

[1] Bald W et al. (2000) Innovative technologies for strip production. Steel Times Int. 24: 16–19.

[2] Cook R, Grocock PG, Thomas PM et al. (1995) Development of the twin-roll casting process. J Mater Proc Technol. 55:76–84.

[3] Fan P, Zhou S, Liang X et al. (1997) Thin strip casting of high speed steels. J Mater Proc Technol 63:792–796.

[4] Park CM, Kim W, Park GJ. (2003) Thermal analysis of the roll in the strip casting process. Mech Res Commun. 30:297–310.

[5] Seo PK, Park K, Kang C. (2004) Semi-solid die casting process with three steps die system. J Mater Proc Technol. 154:442–449.

[6] Watari H, Davey K, Rasgado MT, et al. (2004) Semi-solid manufacturing process of magnesium alloys by twin-roll casting. J Mater Proc Technol. 156:1662–1667.

[7] Hojny M (2017) Modeling of steel deformation in the semi-solid state. Advanced Structured Materials, vol. 78, Springer Switzerland.

[8] Hojny M. (2014) Projektowanie dedykowanych systemów symulacji odkształcania stali w stanie półciekłym. Wzorek, Krakow, Poland.

[9] Pietrzyk M. (1992) Metody numeryczne w przeróbce plastycznej metali. AGH, Krakow.

[10] Glowacki M. (1998) Termomechaniczno-mikrostrukturalny model walcowania w wykrojach kształtowych. AGH, Krakow, Poland.

[11] Yang Z, Sista S et al. (2000) Three dimensional Monte Carlo simulation of grain growth during GTA welding of titanium. Acta Mater. 48:4813–4825.

[12] Monaghan JJ. (1992) Smoothed particle hydrodynamics. Annu Rev Astron Astrophys. 30:543–574.

[13] Monaghan JJ. (1994) Simulating free surface flows with SPH. J Comput Phys. 110: 399–406.

[14] Crespo AAJC et al. (2007) Boundary Conditions Generated by Dynamic Particles in SPH Methods. Cmc—Tech Science Press USA 5:173–184.

[15] Cleary PW, Monaghan JJ. (1999) Conduction modelling using smoothed particle hydrodynamics. J Comput Phys. 148:227–264.

[16] Faqih RA, Naa CF. (2013) Three-dimensional smoothed particle hydrodynamics simulation for liquid metal solidification process. Mater. Proc. ISCS.

[17] Hojny M, Glowacki M. (2011) Modeling of strain-stress relationship for carbon steel deformed at temperature exceeding hot rolling range. J Eng Mater Technol, 133:021008-1–021008-7.